





Cite this: *Polym. Chem.*, 2021, **12**, 2563

Proton conducting ABA triblock copolymers with sulfonated poly(phenylene sulfide sulfone) midblock obtained *via* copper-free thiol-click chemistry†

Marco Viviani, Sebastiaan Pieter Fluitman, Katja Loos  and Giuseppe Portale  *

A series of charged ABA triblock copolymers having sulfonated poly(phenylene sulfide sulfone) (sPSS) as B-block and polystyrene (PS) as A-block have been successfully synthesized using copper-free thiol-click chemistry. One-pot sequential radical addition–fragmentation chain transfer (RAFT) polymerization followed by functionalization with a perfluorinated chain extender (decafluorobiphenyl, DFBP) is used to prepare the PS blocks which are later clicked to the charged sPSS mid-block, synthesized using nucleophilic aromatic substitution polymerization. The proposed synthetic approach ensures good control over the composition of the resulting ABA block copolymers allowing synthesis of block copolymers with well-defined ion exchange capacity (IEC) and nanomorphology. The superstrong segregation regime ($\chi N \gg 100$) of these BCPs generates ordered nanostructures, spanning from spherical to lamellar. All the block copolymers are thermally stable up to 300 °C and are robust against swelling and wetting due to the dimensional stabilization of the ionic domains provided by the PS matrix. The relationship between proton conductivity and nanomorphology is investigated by electrochemical impedance spectroscopy (EIS), revealing the significant impact of self-assembly on the transport properties, reaching a maximum ion conductivity of 50 mS cm^{−1} at 90 °C and 95% RH in the through-plane direction.

Received 22nd January 2021,
Accepted 28th March 2021

DOI: 10.1039/d1py00094b

rsc.li/polymers

Introduction

Green hydrogen production and fuel cell technology, together with electric storage devices (*i.e.* batteries), are expected to lead the energy transition toward renewable sources.^{1–4} Polymer electrolyte (or proton exchange) membrane fuel cells (PEMFC) represent the most efficient devices for energy production combined with a wide range of applications from transportation to portable and stationary power generation.⁵ The key component of these devices is the polymer electrolyte membrane (PEM) which is responsible for the proton transport from the anode to the cathode.

To date, perfluorosulfonic ionomers (PFSI) such as Nafion™, are still the benchmark products and the most used polymers for PEM due to their outstanding proton conductivity at moderate temperatures (0.1 S cm^{−1} at 30 °C and 80% relative humidity (RH))⁶ and chemical stability. Despite modest

ion exchange capacity (IEC), these polymers show unique ion conductivity thanks to the peculiar phase separation between the super-acidic sulfonic group and the tetrafluoroethylene backbone which promotes the development of a percolated densely sulfonated nanostructure.^{7,8} However, thermo-mechanical limitations and high hydration requirements limit the optimal operating temperature below 90 °C.⁹ Moreover, safety and environmental aspects, high fuel crossover and the high cost of production constitute additional problems that prevented the widespread use of PEMFC technology.^{10,11}

To address the aforementioned drawbacks of PFSI membranes, different chemistries mainly based on sulfonated aromatic polymers were investigated as alternative materials for intermediate temperature PEM (70 °C < *T* < 120 °C).^{4,12,13} Particular emphasis was given to the investigation of sulfonated aromatic block copolymers due to their stability and possibility to exploit the self-assembly to tune the nanomorphology, improving PEM performance.^{13–15} Among various factors affecting the stability and the morphologies of the final polymers,^{16–18} the distribution of highly sulfonated segments along the backbone of multiblock copolymers demonstrated the possibility to obtain percolated structures even at low RH.^{15,19,20}

In this regard, sulfonated poly(phenylene sulfide sulfones) (sPSS) represent an interesting class of polymers suitable for

Macromolecular Chemistry and New Polymeric Materials, Zernike Institute for Advanced Materials, University of Groningen, Nijenborgh 4, 9747AG Groningen, The Netherlands. E-mail: g.portale@rug.nl

† Electronic supplementary information (ESI) available: Full details of the experimental protocols with selected spectra and characterization techniques. See DOI: 10.1039/d1py00094b



PEM application.^{21,22} The presence of electron-donating oxygen or sulfur atoms in *ortho* position to the sulfonic group is known to reduce the hydrolytic stability of sulfonated polymers facilitating their desulfonation.^{23,24} However, while ether linkages cannot be oxidized without chain scission, the oxidation of the thioether linkage to sulfone (sPSO2) brings consistent advantages in terms of oxidative and dimensional stability under humidified conditions.^{23,25} Nevertheless, a compromise between IEC and tolerable RH must be considered as excessive swelling or dissolution of the membrane at high IEC are not prevented by simple oxidation of the thioether units.²⁵ The rigidity and high orientation of the $-\text{SO}_2-$ linkage^{26,27} provides additional mechanical strength but also exacerbates the brittleness of the polymers.^{23,28} On the other hand, the sulfide linkage has a shallow rotational barrier that promotes the phase separation of the sPSS and the sulfur atom of the thioether groups can act as an efficient radical scavenger in a fuel cell environment, being readily oxidized to sulfoxide and eventually sulfone in hydrogen peroxide.^{29,30}

Previous works reported the successful implementation of sPSS in multiblock copolymers in combination with different apolar blocks such as poly(arylene ether sulfones)^{31,32} and poly(arylene sulfide nitrile).³³ The obtained results demonstrated superior proton conductivity of the thioether forms compared to the sulfonated analogue.³² However, excessive water uptake affects the performance of the block copolymers at high RH.³² Changing the block copolymer architecture from multiblock to ABA triblock copolymer placing the charged block in the central position has been suggested to prevent excessive swelling and stabilize the ionic domains.^{13,34} So far, this architecture has been barely explored for proton-conducting polymers^{34–38} and only recently ABA structure with aromatic charged midblock have been proposed.³⁶ Synthesis of ABA triblock copolymers requires monofunctional external blocks limiting the choice of aromatic A-blocks to Ni-mediated polymerization of poly(phenylene oxide) (PPO) as reported by Guiver *et al.*³⁴ However, concerning fuel cell applications, metal-catalyzed synthesis poses additional risks as the presence (even in traces) of heavy metals in PEM is known to be detrimental for durability and performance.^{39,40}

To overcome this drawback, we report here a metal-catalyst free approach to synthesize ABA proton conducting triblock copolymers. The copolymers have charged hydrophilic polydisperse sPSS synthesized *via* nucleophilic aromatic substitution polymerization as mid B-block and hydrophobic narrowly dispersed polystyrene (PS) synthesized *via* RAFT polymerization as A-blocks.⁴¹ RAFT polymerization was used here as an ideal platform for metal-free synthesis and thiol-click chemistries.^{42–44} We choose PS here to emphasize the phase separation of the resulting block copolymer (*via* the expected high χ parameter) and, most importantly, because of its good miscibility in polar aprotic solvents such as DMF, DMAc and NMP, that are also good solvents for the sPSS block. Although styrenic polymers are usually not considered ideal materials for PEM, due to their poor oxidative stability,⁴⁵ several works employed PS as model compound in proton conducting

systems^{37,46–48} and others even reported promising oxidative stability⁴⁹ and potential applications.⁵⁰ To avoid metal-catalyzed click-reactions, the blocks were connected using a thiol-fluoro click-chemistry. Decafluorobiphenyl (DFBP) was employed as it readily reacts with thiolate anions under mild conditions^{51,52} and has been reported to improve nanophase separation when used as a linker for sulfonated block copolymers.^{53,54} By varying the molecular weight of the constituting blocks, ABA triblock-copolymers with different compositions and different IEC can be obtained, allowing us to explore the nanostructure–property relationship of this new class of charged block copolymers.

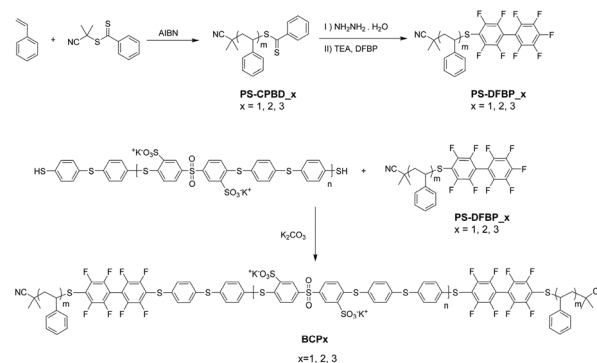
Results and discussion

Three PS-*b*-sPSS-*b*-PS block copolymers have been prepared and studied here. They are named as BCP_x, accordingly to their sPSS content, with $x = 1$ for the lowest sPSS content and $x = 3$ for the highest. The length of the charged sPSS midblock is kept constant, while the length of the hydrophobic PS blocks functionalized with DFBP end-group is varied, which was used in a thiol-fluoro click reaction (Scheme 1). For consistency in the numeration, PS blocks were numbered in the same way of the related BCP (*i.e.* PS1 was used to produce BCP1, *etc.*).

Synthetic procedures

sPSS midblock. sPSS was synthesized following a slightly modified procedure reported in literature.²³ Details about the synthesis and characterization of the sPSS midblock are reported in the ESI.† A special remark is needed for the molecular weight determination of the sPSS *via* GPC analysis. The charged nature of the midblock required a derivatization technique *via* sulfonamide to neutralize the charges and the related interactions with the columns. The proposed method and results are detailed in the ESI.†

One-pot synthesis of PS-DFBP. Decafluorobiphenyl-terminated PS (PS-DFBP) was obtained *via* a “one-pot” sequential



Scheme 1 Synthesis of ABA triblock copolymers based on thiol-fluoro click chemistry. Synthesis of PS-DFBP (top panel) and synthesis of BCP (bottom panel).



functionalization of the PS-CPBD_x ($x = 1, 2, 3$) (Scheme 1, top panel).

The PS blocks were synthesized by radical addition-fragmentation (RAFT) polymerization⁴¹ using 2-cyano-2-propyl benzodithioate (CPBD) as chain transfer agent (CTA). The dry condition of the reaction limited problems related to the sensitivity towards hydrolysis of this class of CTA.⁴² The one-pot sequential functionalization is required to limit the presence of active side-products (*i.e.* alkyl thiols) produced by the aminolysis of trithiocarbonates together with thioureas.⁵⁵ By varying the [CTA]:[Sty] ratio, PS with different molecular weights were synthesized (Table 1). The molecular weight of the resulting polymers was determined by GPC analysis in THF.

The aminolysis with hydrazine⁵⁶ reaction step followed by thiol-halo reaction with decafluorobiphenyl provided the desired PS-DFBP_x ($x = 1, 2, 3$). The disappearance of the characteristic pink color of the polymer solution gave an indication of the progress of the CTA cleavage, whereas UV-Vis spectroscopy confirmed the disappearance of the characteristic absorption peak of the CTA at 306 nm after 30 min at room temperature in DMF (Fig. 1a).

Preliminary experiments in our lab (not reported here) have demonstrated the susceptibility of the DFBP towards nucleophilic substitution by primary amines even at room temperatures in DMF. Hence, a large excess of DFBP and significant dilution was adopted to avoid multiple substitutions of the perfluorinated molecule. This condition ensured the formation of the desired PS-DFBP as confirmed by NMR analysis (Fig. 1b and d).

The ¹H NMR clearly shows the disappearance of the peaks of the *o*-, *p*- and *m*-protons of the CTA phenyl ring at 7.84, 7.66 and 7.48 ppm, respectively (Fig. 1b). Additionally, the signal of the terminal aliphatic proton at 4.85 ppm completely shifts to 4.00 ppm as a result of the substitution of the DFBP group. The ¹⁹F NMR spectrum in CDCl₃ exhibit five different peaks at -134.64, -140.59, -141.74, -153.38 and -163.73 ppm corresponding to the terminal nonafluorobiphenyl group (Fig. 1d). The absence of any other peak confirmed the absence of residual DFBP or multiple substitutions on the fluorinated rings. Despite the oxygen-free atmosphere and the use of hydrazine,⁵⁶ which is known to prevent disulfide formation, a small amount of disulfide coupling occurred as shown by GPC

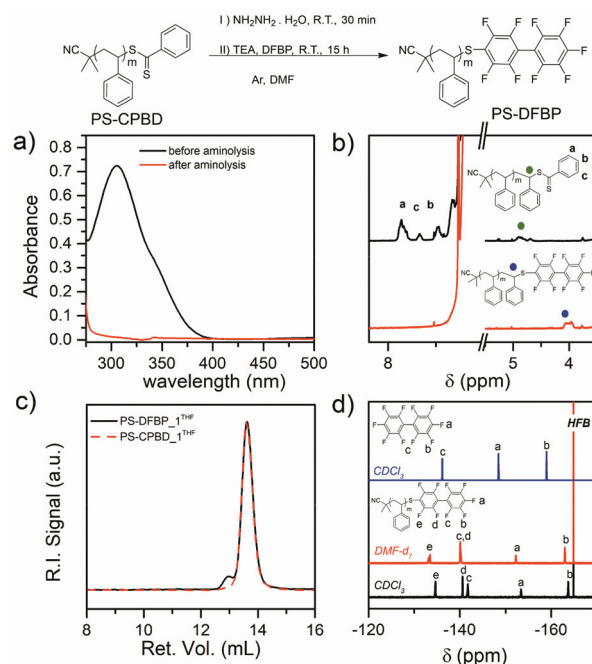


Fig. 1 (a) UV-Vis spectra of PS-CPBD before and after aminolysis (4×10^{-5} M in DMF) showing clear disappearance of CPBD absorption peak at 306 nm. (b) ¹H NMR spectrum of PS-CPBD before and after aminolysis and derivatization with hydrazine and DFBP respectively (PS-DFBP). (c) Comparison of the GPC eluograms of the PS-DFBP₁ and PS-CPBD₁ in THF. (d) ¹⁹F NMR spectra of the DFBP and PS-DFBP the latter in both CDCl₃ and DMF-*d*₇ (hexafluorobenzene was used as reference).

analysis in THF (Fig. 1c) but the dispersity remained low ($D \leq 1.2$) (Table 1) and the formed disulfide did not interfere with the subsequent click reaction.

Synthesis of BCP1, BCP2 and BCP3 via metal-free thiol-fluoro click reaction

The synthesis of BCP_x (with $x = 1, 2$, and 3) was performed in DMF at 50 °C over 4 days under inert atmosphere in the presence of K₂CO₃ as base.^{28,33} Compared to what was reported in literature for the synthesis of multiblock copolymers having DFBP linkers,^{28,31,33} milder conditions were adopted here in order to limit the extent of side reactions (multiple substitutions). An excess of 3 equivalents of PS-DFBP was employed to ensure full conversion of the sPSS end-groups. Residual salts and unreacted PS-DFBP were removed through extensive washing with water and acetone to obtain pure block copolymers. The NMR analysis confirmed the success of the click reaction (Fig. 2a and b).

¹H NMR spectra showed the presence of peaks characteristic of both blocks (Fig. 2a) while ¹⁹F NMR analysis proved the success of the click reaction showing the four main peaks of the octafluorobiphenyl moiety at -133.5, -133.8, -139.2 and -139.8 ppm, respectively (Fig. 2b). Additionally, two minor peaks appeared together with the main signals. Considering the excess of PS-DFBP and the unlikely chemical shifts for the di- and tri-substitution of the DFBP with thiolate anion,⁵³ we

Table 1 Molecular weight characteristics of the pristine PS-CPBD_x ($x = 1, 2$, and 3) and the end-functionalized PS-DFBP_x blocks

X	PS-CPBD _x		PS-DFBP _x	
	M_n^{GPC} ^a (kg mol ⁻¹)	D	M_n^{GPC} ^a (kg mol ⁻¹)	D
1	15.8	1.07	18.0	1.08
2	11.4	1.07	12.3	1.12
3	6.8	1.09	7.5	1.12

^a Obtained by GPC analysis in THF at 35 °C using monodisperse PS standards.



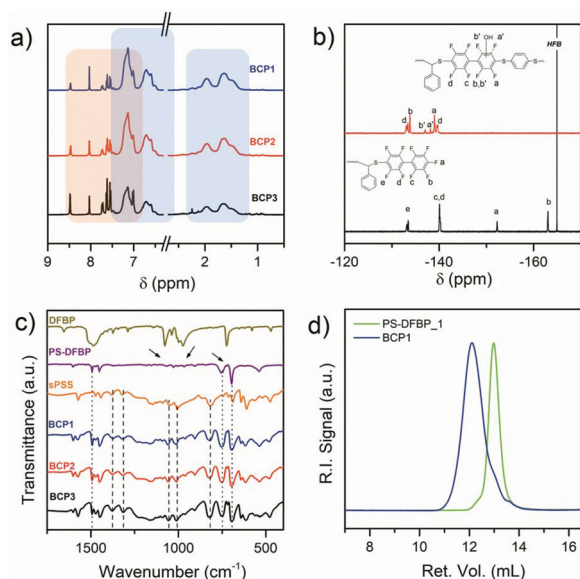


Fig. 2 (a) ^1H NMR of BCP x ($x = 1, 2, 3$) showing the copresence of both the PS and the sPSS peaks highlighted in light blue and light orange, respectively. (b) ^{19}F NMR of the BCP1 in $\text{DMF-}d_7$ showing the conversion of the terminal fluorine of the PS-DFBP into the octafluorobiphenyl unit, the presence of peaks a' and b' is discussed in the main text. (c) FTIR spectra of the BCP x ($x = 1, 2, 3$) showing the presence of the characteristic vibrations of the sPSS (dashed lines) and PS-DFBP (dotted lines) blocks. Black arrows indicate the presence of typical DFBP vibration in the PS-DFBP spectrum confirming the functionalization of the PS block. (d) GPC traces in DMF with 0.01 M LiBr of BCP1 with respective PS-DFBP_1 reported for comparison.

attributed the additional peaks to the presence of hydroxyl-substitution due to moisture absorption under the alkaline environment.

FTIR spectra of the obtained BCPs show the presence of both the sPSS and the PS characteristic vibrations (Fig. 2c). The broad band visible in the range between 1250 and 1140 cm^{-1} is due to the sulfonic group stretching vibrations, while the asymmetric stretching of the $-\text{SO}_2-$ generates the two bands located at 1270 and 1300 cm^{-1} . Additionally, typical signals of poly(*p*-phenylene sulfides)⁵⁷ are present at 1093 , 1074 and 811 cm^{-1} . The $-\text{CH}_2-$ aliphatic stretching from the PS block appear at 1485 cm^{-1} and the monosubstituted benzene out-of-plane deformations at 750 and 730 cm^{-1} . A proportional increase of the sPSS band intensities with its content in the BCP is recognizable (Fig. 2c).

GPC analysis of BCP shows a single peak shifted at lower retention time compared to the PS-DFBP signal, confirming the success of the click reaction (Fig. 2d). Due to the ionic interaction of the BCPs with the column, the molecular weight was calculated based on the wt% composition obtained by ^1H NMR (Table 2) using the molecular weight of the PS obtained by GPC analysis in THF.

The comparison between the compositions of the BCPs calculated based on the M_n obtained by different methods (GPC, ^1H NMR and elemental analysis) are also reported in Table 2. Overall, the agreement between the sPSS fraction measured by the different techniques is good, even though slight discrepancies are observed. These differences might be attributed to partial hydroxy-substitution of the DFBP linker and the possible presence of impurities (*i.e.* alien ions and salts) which are difficult to remove completely in these charged polymers.

Thermal properties

The thermal properties of the BCP in the proton form were analyzed both by DSC and TGA. The results are presented in Fig. 3 and summarized in Table 2. The sPSS homopolymer does not show any T_g up to $250\text{ }^\circ\text{C}$, maximum T explored as the sulfonic group start degrading around $270\text{ }^\circ\text{C}$. Thus, all BCPs show only one glass transition corresponding to the PS blocks and demonstrating strong phase separation between the two blocks. A slight shift to higher temperature is generally observed for the T_g of the PS phase in the BCPs. This is expected due to the rigid nature of the charged block which hinders the free motion of PS chains in the BCP when compared to the homopolymer.

All BCPs possessed good thermal stability with T_d above $300\text{ }^\circ\text{C}$ as demonstrated by TGA (Fig. 3b). A decrease in the T_d was observed with increasing the sPSS. Being the sulfonic group the weakest point in terms of thermal stability, it is possible to observe that in all cases the BCP structure enhanced the overall thermal stability of the material when compared to the pristine sPSS polymer. From Fig. 3b it is also possible to observe that, since the PS-DFBP has negligible residual mass at $700\text{ }^\circ\text{C}$, the residue of BCP x ($x = 1, 2$ and 3) is proportional to the sPSS content. In fact, BCP3 displays the highest residual mass among the block copolymers while BCP1 has the least residue.

Nanostructure characterization

The nanomorphology of the charged block copolymers was studied using TEM and SAXS analysis and the results are sum-

Table 2 Summary of the molecular weight characteristics, composition and thermal properties of the obtained BCPs

	$M_n^{\text{NMR } a}$ (kg mol^{-1})	D	$f_{\text{sPSS}}^{\text{GPC}}$ (wt%)	$f_{\text{sPSS}}^{\text{NMR}}$ (wt%)	$f_{\text{sPSS}}^{\text{EL.An.}}$ (wt%)	$f_{\text{sPSS}}^{\text{NMR } b}$ (vol%)	T_g ($^\circ\text{C}$)	T_d^d ($^\circ\text{C}$)
BCP1	44.1	1.27	16.5	18.4	21.1	13.4	$104.3 (101.5)^c$	336.1
BCP2	32.4	1.29	22.4	24.1	27.6	17.9	$103.3 (100.8)$	328.6
BCP3	26.2	1.36	32.1	42.8	43.9	33.9	$103.4 (96.9)$	316.9

^a Calculated by M_n^{GPC} values of PS taking into account the wt% composition of block copolymers obtained by ^1H NMR analysis. ^b Evaluated from the wt% considering the density of the pristine polymers ($\rho_{\text{PS}} = 1.05\text{ g cm}^{-3}$ (ref. 61) and $\rho_{\text{sPSS}} = 1.53\text{ g cm}^{-3}$ (ref. 23)) and neglecting the mixing effects. ^c Values in brackets represent T_g values of corresponding pristine PS-DFBP $_x$ ($x = 1, 2, 3$). ^d Temperature corresponding to the 5 wt% weight loss.



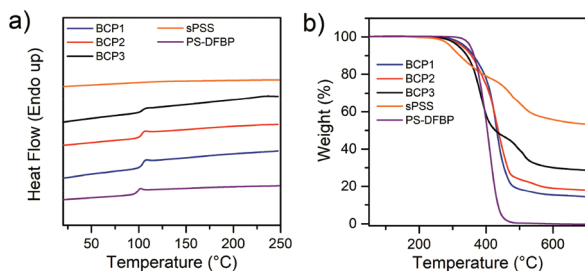


Fig. 3 (a) DSC thermograms of the block copolymers recorded during the second heating run at $10\text{ }^{\circ}\text{C min}^{-1}$ under nitrogen atmosphere, the traces of PS-DFBP and sPSS are reported for comparison. (b) TGA thermograms of the block copolymers recorded at $10\text{ }^{\circ}\text{C min}^{-1}$ under nitrogen atmosphere, both PS-DFBP and sPSS thermograms are reported for comparison.

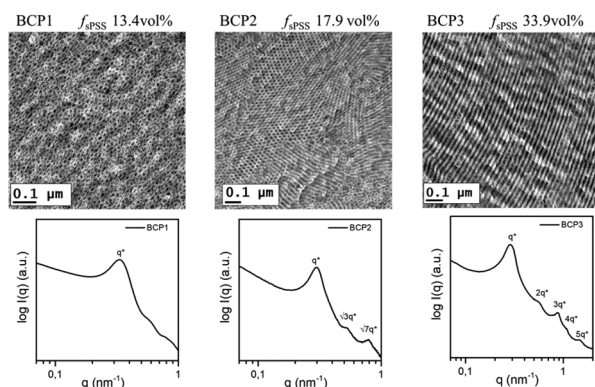


Fig. 4 TEM images of the BCP stained with Cs^+ ions and the corresponding SAXS profiles obtained from the H-form (BCP1 and BCP3) and Cs-form (BCP2) of the dried membranes at room temperature.

marized in Fig. 4 and Table 3. Membranes cast from DMAc and ion-exchanged with H^+ or Cs^+ were analyzed. Cs^+ was used here to enhance the contrast of the ionic domains due to the higher electron density of the Cs^+ ions with respect to H^+ . The effect of the linker between the blocks on the self-assembly of sulfonated aromatic polymers has been reported,^{28,53,54} with perfluorinated linkers promoting the formation of better phase-separated morphologies. As a result of the rigidity of the sPSS block and of the DFBP linker, a slow casting protocol ($40\text{ }^{\circ}\text{C}$ for 3 days) from solutions with dilution below 10 wt% was required to develop well-defined nanostructures.⁵⁸

All BCPs show enhanced phase separation as a result of the strong incompatibility between the PS and the charged sPSS blocks. For classical block copolymers with strong phase segre-

gation, different morphologies are expected depending on the volume fraction of the B-block.⁵⁹ For the BCP1 ($f_{\text{sPSS}} = 13.4\text{ vol\%}$), a spherical structure was observed with a periodicity of $d = 2\pi/q^* = 19\text{ nm}$ and an average radius of 9.2 nm (estimated using the position of the minima in the SAXS curve and fitting of the SAXS curve, not showed here). SAXS and TEM analysis of BCP2 and BCP3 revealed the existence of two different morphologies. BCP2 ($f_{\text{sPSS}} = 17.9\text{ vol\%}$) showed formation of hydrophilic cylindrical domains with a SAXS peak sequence typical for the hexagonally packed morphology⁶⁰ at $q^* : \sqrt{3}q^* : \sqrt{7}q^*$ and with a domain spacing $d = 2\pi/q^* = 21\text{ nm}$ ($q^* = 0.30\text{ nm}^{-1}$).

Highly oriented lamellar structures already appeared at $f_{\text{sPSS}} = 33.9\text{ vol\%}$ in BCP3. SAXS pattern of BCP3 exhibits scattering maxima at $q^*, 2q^*, 3q^*, 4q^*$ and $5q^*$ that correspond to the (100), (200), (300), (400) and (500) scattering reflections of a lamellar structure.

To evaluate the extent of incompatibility between the PS and sPSS blocks, a χ parameter estimation was attempted based on the lamellar spacing of the BCP3 using the formalism developed for monodisperse block-copolymers⁶³ (eqn (1)):

$$\chi = \left(\frac{d_{\text{LAM}} \sqrt{6}}{aN_{\text{di}}^{2/3}} \left(\frac{\pi^2}{3} \right)^{1/3} \right)^6 = \left(\frac{d_{\text{LAM}}}{1.1aN_{\text{di}}^{2/3}} \right)^6 \quad (1)$$

where a is the volume fraction weighted root-mean-square average of the statistical segment lengths, $a = (a_{\text{sPSS}}^2 \times f_{\text{sPSS}} + a_{\text{PS}}^2 \times (1 - f_{\text{sPSS}}))^{\frac{1}{2}}$ and $N_{\text{di}} = N_{\text{tot}}/2$ is the equivalent diblock degree of polymerization. The results obtained considering the room temperature parameters for BCP3 provided χ values of 2.73 with corresponding χN of ca. 360.

Similar conclusions can be obtained considering the Hildebrand's solubility parameters estimation (eqn (2)) in combination with the concepts of regular solution theory⁶⁴ that allows expression of the χ parameter for a couple of homopolymers A and B as:

$$\chi_{\text{AB}} = \frac{\nu}{kT} (\delta_{\text{A}} - \delta_{\text{B}})^2 \quad (2)$$

wherein ν is a reference molar volume of $118\text{ }^{\circ}\text{A}^3$, k is the Boltzmann constant, T is the absolute temperature, δ_{A} and δ_{B} are the solubility parameter of the homopolymer A (PS) and B (sPSS), respectively. We estimated the δ_i contribution using the approximation proposed by Fedors⁶⁴ from tabulated cohesive parameters⁶¹ according to eqn (3).

$$\delta_i = \left(\frac{\Delta E_i^v}{V_i} \right)^{\frac{1}{2}} = \left(\frac{\sum_j n_j \Delta e_j}{V_i} \right)^{\frac{1}{2}} \quad (3)$$

where n_j is the number of groups present in the repeating unit of the polymer, Δe_j is the cohesive energy of each group and V_i is the group molar volume. Although there is a lack of specific parameters for all of the functional groups present in our macromolecules, a good agreement is found here between the SAXS values (≈ 2.73) and the group solubility parameter esti-

Table 3 Block copolymer compositions and characteristic dimensions obtained from SAXS analysis

	f_{sPSS} (vol%)	f_{PS} (vol%)	q^* (nm^{-1})	d (nm)	Morph
BCP1	13.4	86.6	0.33	19.0	SPH
BCP2	17.9	82.1	0.30	21.0	CYL
BCP3	33.9	66.1	0.27	23.9	LAM



mation (≈ 2.36). Even if the estimated value of χ presented here should be considered with care, as the equations used for the estimation have been derived for non-charged polymers, these numbers suggest that the synthesized ABA block copolymers reside in a superstrong segregation regime having $\chi N \gg 100$.⁶⁵

Dimensional stabilization upon hydration

Generally, our PS-*b*-sPSS-*b*-PS BCPs were brittle at ambient temperature. However, for BCP1, BCP2 and BCP3, membranes could be obtained and exposed to water vapour or immersed in water, allowing the investigation of the swelling effect on their ionic domain sizes.

A medium angle X-ray scattering (MAXS) study of the ionomer peak position in the BCP and the sPSS was performed (Fig. 5). All BCPs show a distinct ionomer peak in the dry state ($q_{\text{ion}}^* \approx 3.3 \text{ nm}^{-1}$, $d_{\text{ion}} \approx 1.9 \text{ nm}$) with a peak position similar to the sPSS homopolymer ($q_{\text{ion}}^* = 3.65 \text{ nm}^{-1}$, $d_{\text{ion}} = 1.7 \text{ nm}$).

This suggests that the hydrophilic chains preserve their native packing inside the BCP domains. However, under humidified conditions, the three BCPs behave differently. Generally, the ionomer peak position in the BCP shifts to lower q (increase in domain size), but the shift is definitively smaller than the one observed for the sPSS which swells excessively at the limit of dissolution. An ionic domain enlargement below 75% was observed for all the BCPs, sensibly lower if compared to the 123% of the pure sPSS. Thus, the BCP structure greatly reduces the dimensional change in the ionic domain size, with the PS scaffold preventing dissolution but

not preventing water molecules to penetrate the sPSS domains and facilitating the hydration of the sulfonic groups.

Further details about the hierarchical structure in these materials can be learned by observation of the 2D X-ray patterns. Interestingly, in the case of BCP3 possessing LAM nanostructure, the MAXS/SAXS pattern clearly shows a strong orthogonal orientation of the ionomer peaks against the lamellar ones (Fig. 5c, inset).

This means that the ionic pathways are orthogonally oriented with respect to the lamellar domains as depicted in Fig. 5d. Our observation further shades light on the structure of sPSS systems that is not well studied so far. Due to the semi-rigid sPSS chain conformation, the ionomer peak directly relates to the interchain distance of adjacent sPSS chain segments. This means that the sPSS chains are highly oriented and self-organized perpendicular to the lamellae directions with ionic groups forming narrow channels perpendicular to the PS “walls”.

This kind of organization might be facilitated here by the stiffness of both the sPSS and the DFBP linker that induced a stretched conformation in the sPSS chains between the PS domains, forcing spontaneous structure alignment during membrane formation. Another interesting observation is that, while for the BCP2 and BCP1 the ionomer peak decreases in intensity upon swelling (suggesting humidity-induced disordering), for BCP3 the ionomer peak intensity is enhanced upon water absorption, as observed for pure sPSS. This means that the peculiar orthogonal arrangement of the sPSS chains with respect to the lamellar planes, favors swelling without compromising the high degree of order of the LAM structure. This is not the case for nanomorphologies with curved interfaces (spherical and cylindrical).

Oxidative stability and proton conductivity

The oxidative stability of the BCP was evaluated using an accelerated test by immersing pieces of membranes for 1 h at 80 °C in Fenton's reagent and the results are reported in Table 4. Interestingly, the highest degradation was observed for the BCP3 that contained the highest weight fraction of sPSS. This might be explained considering the higher hydrophilicity of BCP3 compared to BCP1 and BCP2 that facilitated the reagent penetration inside the membrane. On the contrary, the hydrophobicity induced by the higher content of PS in BCP1 and BCP2 limited the degradation within the considered time interval most probably due to limited mass transfer of the reagent inside the membrane.

The proton conductivity of these sulfonated polymers is strongly dependent on their ion exchange capacity (IEC). This parameter could be retrieved by back titration of the exchanged proton ions in a salt solution or by evaluation of the ^1H NMR composition. The results obtained for BCP1, BCP2 and BCP3 are summarized in Table 4 confirming the increasing trends with increasing sPSS fractions. Generally, an underestimation of the IEC values determined by titration if compared with the value obtained by ^1H NMR is observed. This could be ascribed to the limited availability of some

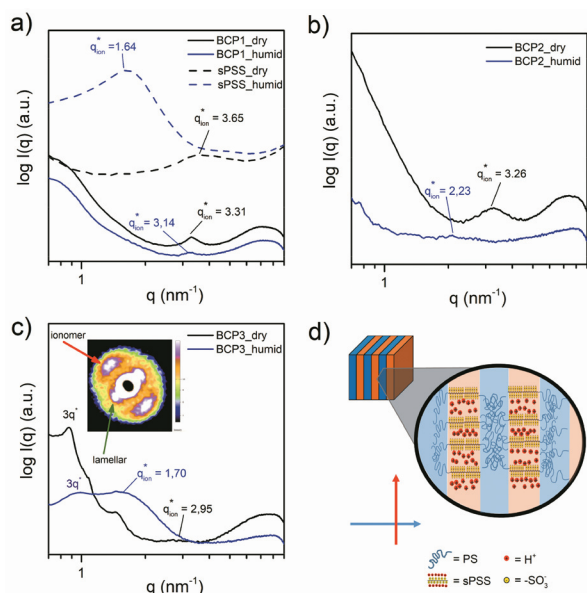


Fig. 5 MAXS profile at room temperature under dry and hydrated conditions (RH 95%) of (a) BCP1 and sPSS, (b) BCP2 and (c) BCP3 in their protonated form. Inset in (c) quadrant represent the 2D MAXS pattern showing the orthogonal orientation of the ionomer peak with respect to the lamellar direction. (d) Cartoon representing the relative orientation of the lamellae and the ionic domains inside BCP3.



Table 4 Ion exchange capacity, water uptake and nanoscale swelling of BCP1, BCP2 and BCP3

	Morph	IEC ^{titr.} ^a (meq g ⁻¹)	IEC ^{NMR} ^b (meq g ⁻¹)	W.U. ^c (%)	λ ([H ₂ O]/[SO ₃ H])	R.W. ^d (%)	$\Delta d/d_{\text{dry}}$ (%)
sPSS	—	3.18	—	—	—	—	123
BCP1	SPH	0.32	0.58	3.0	5	97.1	5.3
BCP2	CYL	0.60	0.79	10.2	9	89.9	50
BCP3	LAM	1.31	1.36	28.7	12	54.5	74

^a Obtained from titration with NaOH 0.01 N. ^b Calculated from ¹H NMR composition. ^c Evaluated after immersion in water at 25 °C for 24 h.

^d Residual weight after 1 h immersion in Fenton's reagent at 80 °C.

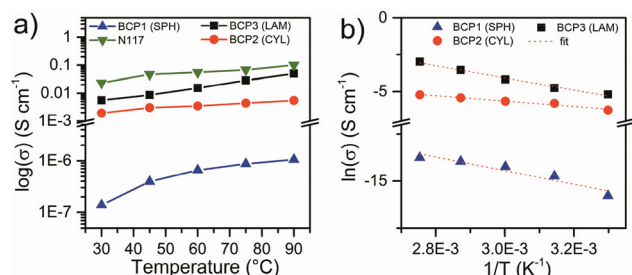


Fig. 6 (a) Through-plane proton conductivity of BCP1 BCP2, BCP3 and Nafion™ N117 at 95% RH as a function of temperature. (b) Arrhenius plot of proton conductivity for BCPs.

–SO₃H groups for the H⁺/Na⁺ exchange⁶⁶ in the spherical and cylindrical structures.

The proton conductivity of the selected BCPs was measured in the through-plane direction at 95% RH as a function of temperature between 30 and 90 °C (Fig. 6). As it was not possible to obtain large (cm²) membranes for some of the BCPs, stacks of membrane slices were pelletized and measured in order to investigate in a comparable manner the effect of nanomorphology on the conductivity on all the BCPs.

As expected, the proton conductivity increases with increasing sPSS wt% fraction and temperature. In addition, comparing the results obtained for the three selected BCPs, the dramatic impact of the nanomorphology on the macroscopic proton transport properties is evident. Considering the values at 90 °C, an increase of about 6 wt% of sPSS between BCP2 (CYL) and BCP1 (SPH) generates an increase of more than four orders of magnitude in conductivity. In contrast, a limited increase in conductivity was observed for BCP3 considering the ~18 wt% increase in f_{sPSS} . These observations can be directly ascribed to the nanostructural features of the block copolymers and also to the limited water uptake of the BCP1 compared to the other two BCPs (Table 4). The spherical morphology of BCP1 has a very low degree of percolation with the ionic domains confined by the PS matrix in closed spheres. Moreover, the limited WU provides minimal hydration level (λ), close to the limit of proton dissociation⁸ which explains the low conductivity registered. On the other hand, the presence of elongated channels and interconnections between the hydrophilic cylinders in BCP2 (Fig. 4) is primarily responsible for the improved proton conductivity. Additionally, the λ increase corroborates the MAXS observation and the higher

accessibility of water to the ionic domains. When it comes to the lamellar structure, considering the difference in sPSS content between BCP2 and BCP3, a large increase in proton conductivity was expected. The relatively low increase in proton conductivity observed here can be rationalized considering that the orientation of a non-negligible portion of the lamellar structures, even if partially randomized in the stack, is orthogonal to the through-plane direction. For the aforementioned reasons, the highest conductivity value measured is about 50 mS cm⁻¹ at RH 95% and 90 °C. This is in the same order of magnitude but lower with respect to the benchmark Nafion™ N117 tested in the same conditions (Fig. 6a). A conductivity test for BCP3 in fully wet conditions at 30 °C provided a conductivity of 20 mS cm⁻¹ which is approximately 4 times higher than the same polymer at 95% RH and comparable to the value obtained at 80 °C (95% RH). This result confirmed the relevance of hydration for proton conductivity in sulfonated block copolymers and the potential of these ABA block copolymers under fully wet conditions.

The proton conductivity values exhibited by our BCP3 (LAM) sample are in the same range, yet slightly lower, than other ABA copolymers with charged mid B-block reported recently in literature by Agudelo *et al.*³⁶ The difference in conductivity is most probably due by the fact that in ref. 36 the samples have been measured in the fully hydrated state, while our tests were conducted at RH = 95%. Interestingly, a stronger influence of the rigidity of the A-block on the conductivity compared to the influence of the IEC values was reported.³⁶ Similarly, in our case the “glassy” state of the PS block is responsible for the modest conductivity values obtained. Arrhenius plot of proton conductivity (Fig. 6b) shows a linear dependence of the proton conductivity on temperature with activation energies between 16 and 35 eV, comparable to sulfonated poly(phenylene sulfone) copolymers with similar hydration level.⁶⁷

Conclusions

In this work, we introduced a strategy to synthesize proton conducting ABA triblock copolymers with charged sulfonated midblock flanked by narrowly dispersed polystyrene blocks using copper-free “thiol-click” chemistry. This approach provides unique flexibility and control over the composition and the resulting nanomorphology of the block copolymers and



overcomes problems related to the presence of alien metal ions used in common click chemistry without sacrificing control over the block copolymer architecture.

A decafluorobiphenyl-functionalized PS was reacted with thiol terminated sPSS to give ABA triblock copolymers. In all cases, insoluble membranes were obtained when $f_{\text{sPSS}}^{\text{vol}} < 50\%$, thus eliminating problems related to sPSS water solubility. All the BCPs possessed high thermal stability with T_d around 300 °C. Nanostructure analysis *via* X-ray scattering techniques and TEM clearly show strong phase-separation with achievement of ordered nanostructures. Spherical, cylindrical and lamellar nanomorphologies appeared depending on the block copolymer composition. X-ray scattering analysis of the ionomer peak revealed a strong reduction in the swelling of the nanostructure (75% in the case of the lamellar BCP3 compared to 123% of the sPSS) as a result of the dimensional stabilization of the ionic domains provided by the hydrophobic PS matrix. Proton conductivity tested in the through-plane direction revealed the relevance of the nanomorphology on the proton transport, exhibiting Arrhenian behavior and activation energies typically in the range of other sulfonated aromatic polymers. Although further improvements are required in terms of membrane preparation and proton conductivity at reduced humidity, the highest value of 50 mS cm⁻¹@RH95%, 90 °C measured here for the lamellar structure is promising for future applications in polymer membrane fuel cells. Moreover, these strongly phase separated systems could be interesting in the future to produce sensors and other electro-active devices, especially if we consider that some of them show tendency to spontaneous anisotropic alignment of the nanostructure at the macroscopic scale.

Author contributions

The manuscript was written through contributions of all authors. The concept of the project was developed by M. Viviani and G. Portale. Experimental work was conducted by M. Viviani and S.P. Fluitman. Data interpretation and drafting of the manuscript was conducted by M. Viviani and G. Portale. The manuscript was edited by M. Viviani, K. Loos and G. Portale. All authors have given approval to the final version of the manuscript.

Conflicts of interest

There are no conflicts to declare.

Acknowledgements

The authors acknowledge Albert J. J. Woortman for GPC analysis, Jur van Dijken for the TGA measurements and Ir. Johans van der Velde for the elemental analysis. G. P. acknowledges the Zernike Institute for Advanced Materials for the startup funding that was used to finance this project.

Notes and references

- 1 Y. Ding, Z. P. Cano, A. Yu, J. Lu and Z. Chen, *Electrochem. Energy Rev.*, 2019, **2**, 1–28.
- 2 Z. Ma, D. R. MacFarlane and M. Kar, *Batteries Supercaps*, 2019, **2**, 115–127.
- 3 S. Muench, A. Wild, C. Friebe, B. Häupler, T. Janoschka and U. S. Schubert, *Chem. Rev.*, 2016, **116**, 9438–9484.
- 4 A. Kraysberg and Y. Ein-Eli, *Energy Fuels*, 2014, **28**, 7303–7330.
- 5 The US Department of Energy (DOE), *Fuel Cell Technol. Off.*, 2016, **2015**, 1–58.
- 6 C. Ma, L. Zhang, S. Mukerjee, D. Ofer and B. Nair, *J. Membr. Sci.*, 2003, **219**, 123–136.
- 7 K. A. Mauritz and R. B. Moore, *Chem. Rev.*, 2004, **104**, 4535–4586.
- 8 K.-D. Kreuer, S. J. Paddison, E. Spohr and M. Schuster, *Chem. Rev.*, 2004, **104**, 4637–4678.
- 9 K.-D. Kreuer, *Chem. Mater.*, 2014, **26**, 361–380.
- 10 M. Rikukawa and K. Sanui, *Prog. Polym. Sci.*, 2000, **25**, 1463–1502.
- 11 R. Dams and K. Hintzer, *Fluorinated Polymers: Applications*, Royal Society of Chemistry, 2017, ch. 1, vol. 2, pp. 1–30.
- 12 H. Zhang and P. K. Shen, *Chem. Rev.*, 2012, **112**, 2780–2832.
- 13 D. W. Shin, M. D. Guiver and Y. M. Lee, *Chem. Rev.*, 2017, **117**, 4759–4805.
- 14 N. Li and M. D. Guiver, *Macromolecules*, 2014, **47**, 2175–2198.
- 15 Y. A. Elabd and M. A. Hickner, *Macromolecules*, 2011, **44**, 1–11.
- 16 G. He, Z. Li, J. Zhao, S. Wang, H. Wu, M. D. Guiver and Z. Jiang, *Adv. Mater.*, 2015, **27**, 5280–5295.
- 17 T. J. Peckham and S. Holdcroft, *Adv. Mater.*, 2010, **22**, 4667–4690.
- 18 K. Goto, I. Rozhanskii, Y. Yamakawa, T. Otsuki and Y. Naito, Award ACCOUNTS SPSJ Award Accounts, *Polym. J.*, 2009, **41**, 95–104.
- 19 K. Nakabayashi, K. Matsumoto and M. Ueda, *J. Polym. Sci., Part A: Polym. Chem.*, 2008, **46**, 3947–3957.
- 20 K. Nakabayashi, K. Matsumoto, T. Higashihara and M. Ueda, *J. Polym. Sci., Part A: Polym. Chem.*, 2008, **46**, 7332–7341.
- 21 F. Wang, J. Mechem, W. Harrison and J. E. McGrath, in *American Chemical Society, Polymer Preprints, Division of Polymer Chemistry*, 2000, vol. 41, pp. 1401–1402.
- 22 K. B. Wiles, I. A. Bhanu, F. Wang and J. E. McGrath, in *American Chemical Society, Polymer Preprints, Division of Polymer Chemistry*, 2002, vol. 43, pp. 993–994.
- 23 M. Schuster, K.-D. D. Kreuer, H. T. Andersen and J. Maier, *Macromolecules*, 2007, **40**, 598–607.
- 24 S. Takamuku and P. Jannasch, *Polym. Chem.*, 2012, **3**, 1202–1214.
- 25 M. Schuster, C. C. De Araujo, V. Atanasov, H. T. Andersen, K. D. Kreuer and J. Maier, *Macromolecules*, 2009, **42**, 3129–3137.



- 26 I. Baxter, A. Ben-Haida, H. M. Colquhoun, P. Hodge, F. H. Kohnke and D. J. Williams, *Chem. – Eur. J.*, 2000, **6**, 4285.
- 27 H. M. Colquhoun, P. L. Aldred, F. H. Kohnke, P. L. Herbertson, I. Baxter and D. J. Williams, *Macromolecules*, 2002, **35**, 1685–1690.
- 28 G. Titvinidze, K.-D. Kreuer, M. Schuster, C. C. de Araujo, J. P. Melchior and W. H. Meyer, *Adv. Funct. Mater.*, 2012, **22**, 4456–4470.
- 29 S. Y. Lee, N. R. Kang, D. W. Shin, C. H. Lee, K.-S. S. Lee, M. D. Guiver, N. Li and Y. M. Lee, *Energy Environ. Sci.*, 2012, **5**, 9795–9802.
- 30 D. Zhao, J. Li, M. K. Song, B. Yi, H. Zhang and M. Liu, *Adv. Energy Mater.*, 2011, **1**, 203–211.
- 31 F. Schönberger, M. Hein and J. Kerres, *Solid State Ionics*, 2007, **178**, 547–554.
- 32 S. Takamuku and P. Jannasch, *Macromolecules*, 2012, **45**, 6538–6546.
- 33 D. W. Shin, S. Y. Lee, C. H. Lee, K.-S. Lee, C. H. Park, J. E. McGrath, M. Zhang, R. B. Moore, M. D. Lingwood, L. A. Madsen, Y. T. Kim, I. Hwang and Y. M. Lee, *Macromolecules*, 2013, **46**, 7797–7804.
- 34 N. Li, S. Y. Lee, Y.-L. Liu, Y. M. Lee and M. D. Guiver, *Energy Environ. Sci.*, 2012, **5**, 5346–5355.
- 35 M. L. Disabb-Miller, Z. D. Johnson and M. A. Hickner, *Macromolecules*, 2013, **46**, 949–956.
- 36 N. A. Agudelo, J. Palacio and B. L. López, *J. Mater. Sci.*, 2019, **54**, 4135–4153.
- 37 T. Saito, H. D. Moore, M. A. Hickner, H. D. Moore and M. A. Hickner, *Macromolecules*, 2010, **43**, 599–601.
- 38 Z. Shao, A. Sannigrahi and P. Jannasch, *J. Polym. Sci., Part A: Polym. Chem.*, 2013, **51**, 4657–4666.
- 39 A. Collier, H. Wang, X. Zi Yuan, J. Zhang and D. P. Wilkinson, *Int. J. Hydrogen Energy*, 2006, **31**, 1838–1854.
- 40 X. Cheng, Z. Shi, N. Glass, L. Zhang, J. Zhang, D. Song, Z.-S. Liu, H. Wang and J. Shen, *J. Power Sources*, 2007, **165**, 739–756.
- 41 J. Chiefari, Y. K. B. Chong, F. Ercole, J. Krstina, J. Jeffery, T. P. T. Le, R. T. A. Mayadunne, G. F. Meijs, C. L. Moad, G. Moad, E. Rizzardo and S. H. Thang, *Macromolecules*, 1998, **31**, 5559–5562.
- 42 S. Perrier, *Macromolecules*, 2017, **50**, 7433–7447.
- 43 P. J. Roth, C. Boyer, A. B. Lowe and T. P. Davis, *Macromol. Rapid Commun.*, 2011, **32**, 1123–1143.
- 44 D. P. Nair, M. Podgórski, S. Chatani, T. Gong, W. Xi, C. R. Fenoli and C. N. Bowman, *Chem. Mater.*, 2013, **26**, 724–744.
- 45 M. A. Hickner, H. Ghassemi, Y. S. Kim, B. R. Einsla and J. E. McGrath, *Chem. Rev.*, 2004, **104**, 4587–4612.
- 46 L. Rubatat, Z. Shi, O. Diat, S. Holdcroft and B. J. Frissen, *Macromolecules*, 2006, **39**, 720–730.
- 47 Z. Shi and S. Holdcroft, *Macromolecules*, 2005, **38**, 4193–4201.
- 48 A. C. C. Yang, R. Narimani, B. J. Frissen and S. Holdcroft, *J. Membr. Sci.*, 2014, **469**, 251–261.
- 49 Y. Tamura, L. Sheng, S. Nakazawa, T. Higashihara and M. Ueda, *J. Polym. Sci., Part A: Polym. Chem.*, 2012, **50**, 4334–4340.
- 50 A. Oishi, H. Matsuoka, T. Yasuda and M. Watanabe, *J. Mater. Chem.*, 2009, **19**, 514–521.
- 51 S. Alapour, B. G. De La Torre, D. Ramjugernath, N. A. Koorbanally and F. Albericio, *Bioconjugate Chem.*, 2018, **29**, 225–233.
- 52 C. Langner, J. Meier-Haack, B. Voit and H. Komber, *J. Fluor. Chem.*, 2013, **156**, 314–321.
- 53 A. S. Badami, O. Lane, H.-S. Lee, A. Roy and J. E. McGrath, *J. Membr. Sci.*, 2009, **333**, 1–11.
- 54 H.-S. Lee, A. Roy, O. Lane, S. Dunn and J. E. McGrath, *Polymer*, 2008, **49**, 715–723.
- 55 X.-P. Qiu and F. M. Winnik, *Macromol. Rapid Commun.*, 2006, **27**, 1648–1653.
- 56 W. Shen, Q. Qiu, Y. Wang, M. Miao, B. Li, T. Zhang, A. Cao and Z. An, *Macromol. Rapid Commun.*, 2010, **31**, 1444–1448.
- 57 D. A. Zimmerman, J. L. Koenig and H. Ishida, *Spectrochim. Acta, Part A*, 1995, **51**, 2397–2409.
- 58 M. Lee, J. K. Park, H.-S. Lee, O. Lane, R. B. Moore, J. E. McGrath and D. G. Baird, *Polymer*, 2009, **50**, 6129–6138.
- 59 M. W. Matsen and F. S. Bates, *Macromolecules*, 1996, **29**, 1091–1098.
- 60 W. Takagi, J. Suzuki, Y. Aoyama, T. Mihira, A. Takano and Y. Matsushita, *Macromolecules*, 2019, **52**, 6633–6640.
- 61 J. Brandrup, E. H. Immergut and E. A. Grulke, *Polymer Handbook*, Wiley & Sons Inc., 4th edn, 2003.
- 62 M. J. Park and N. P. Balsara, *Macromolecules*, 2008, **41**, 3678–3687.
- 63 M. W. Matsen and F. S. Bates, *J. Chem. Phys.*, 1997, **106**, 2436–2448.
- 64 R. F. Fedors, *Polym. Eng. Sci.*, 1974, **14**, 472–472.
- 65 K. P. Mineart, B. Lee and R. J. Spontak, *Macromolecules*, 2016, **49**, 3126–3137.
- 66 K. Krajcinovic, T. Kaz, T. Haering, V. Gogel and J. Kerres, *Fuel Cells*, 2011, **11**, 787–800.
- 67 C. C. de Araujo, K. D. Kreuer, M. Schuster, G. Portale, H. Mendil-Jakani, G. Gebel and J. Maier, *Phys. Chem. Chem. Phys.*, 2009, **11**, 3305–3312.

